

Project: **620**

Project title: **Vertical Propagation of Gravity Waves into the Middle Atmosphere**

Project lead: **Andreas Dörnbrack**

Report period: **2018-01-01 to 2018-12-31**

In the reporting period, the computer time was mainly used to conduct simulations of mountain wave events which were observed during the GW-LCYCLE2 campaign (“Investigation of the life cycle of gravity waves (GW-LCYCLE)” (PI: M. Rapp) in the BMBF-initiative ROMIC¹). The simulations are tied closely to the atmospheric conditions encountered during the field measurements. This strategy enabled the interpretation of measurement data by means of involved important processes. The first part of this report presents numerical simulations conducted for an observed stall warning event of the High Altitude and Long Range Research Aircraft (HALO) over the Apennines in Italy (Bramberger et al., 2018). The physical conditions that led to a series of stall warnings are investigated. The second part of this report focuses on trapped and non-hydrostatic gravity waves in the tropopause region and how they are represented in airborne measurements. Simulations for realistic background conditions and topography were conducted for a mountain wave event over Southern Scandinavia which was observed by coordinated measurements of HALO and the DLR Falcon research aircraft.

HALO stall warning event

The stall warnings at flight level 410 (12.5 km) occurred unexpectedly and the dangerous flight situation was mitigated by pilot intervention. At the incident location, the stratosphere was characterized by large horizontal variations in the along-track wind speed and temperature. On this particular day, strong north-westerly winds in the lower troposphere in concert with an aligned polar front jet favoured the excitation and vertical propagation of large-amplitude mountain waves at and above the Apennines in Italy. These mountain waves carried large vertical energy fluxes of 8 W/m^2 and propagated without significant dissipation from the troposphere into the stratosphere. While turbulence is a well-acknowledged hazard to aviation, this case study reveals that nonbreaking, vertically propagating mountain waves also pose a potential hazard, especially to high-flying aircraft. It is the wave-induced modulation of the ambient along-track wind speed that may decrease the aircraft speed toward the minimum needed stall speed.

To assess the magnitude of mountain wave-induced perturbations above the Apennines, we conducted high-resolution, quasi-realistic numerical simulations with the multiscale geophysical flow solver EULAG (Prusa et al. 2008). For this analysis, a time period was selected after a quasi-steady state of the numerical integrations was achieved. The computational grid was centred on the stall-warning event (see Fig. 1) and comprises $336 \times 240 \times 76$ grid points in the zonal, meridional, and vertical directions, respectively.

¹ ROMIC: *Role of the middle atmosphere in climate*, a research initiative funded by the German Ministry for Education and Research.

The horizontal resolution is 2.5 km, the vertical resolution is 500 m, and the time step is 5 s. The topography is the global relief model (ETOPO1; Amante and Eakins 2009) (see Fig. 1) with a horizontal resolution of 1 arc min which is linearly interpolated onto the computational grid of EULAG.

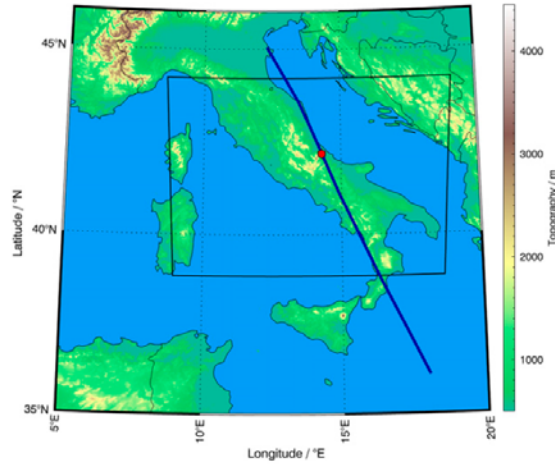


Fig. 1: Flight track above Italy (dark-blue line). The red circle shows the location of the stall warnings, and the box outlined in black displays the computational domain of the EULAG simulations. Flight direction was from north to south. The topography is the global relief model ETOPO1 and also was used in the high-resolution numerical simulations.

The initial and boundary conditions of horizontal wind speed and potential temperature are given by single profiles of each, extracted from ECMWF spectrally truncated data up to wavenumber 21 (T21). These profiles are a zonal mean from 10° to 11.5 °E taken upstream of the stall-warning event at 42°N and 0600 UTC. Figure 2 shows the horizontal wind profile that was used as input for EULAG. The initialization with a single, hydrostatically balanced state neglects large-scale meridional gradients such as the change in tropopause altitude. However, all perturbations can be attributed to the applied forcing of the flow across the Apennines. In the following and in the context of the EULAG simulations, perturbations are defined as the deviation from the initial conditions. Because of the idealized approach of these simulations, one cannot expect to find a one by one agreement between the in situ measurements and the simulations. We aim instead at understanding whether vertically propagating mountain waves can induce wind and temperature perturbations at flight level and on horizontal scales comparable to the observations.

The EULAG simulations reveal coherent, stationary structures in the perturbations of the potential temperature as well as the meridional and vertical wind fields above Italy (Figs. 3a–c). The simulations also indicate that mountain waves with larger horizontal wavelengths dominate the meridional wind and temperature perturbations, while smaller-scale mountain waves prevail in the vertical wind. Amplitudes in the meridional wind field are about 9 m/s; amplitudes are about 4 m/s in the vertical wind speed. The perturbations of the potential temperature reach values of up to 7 K.

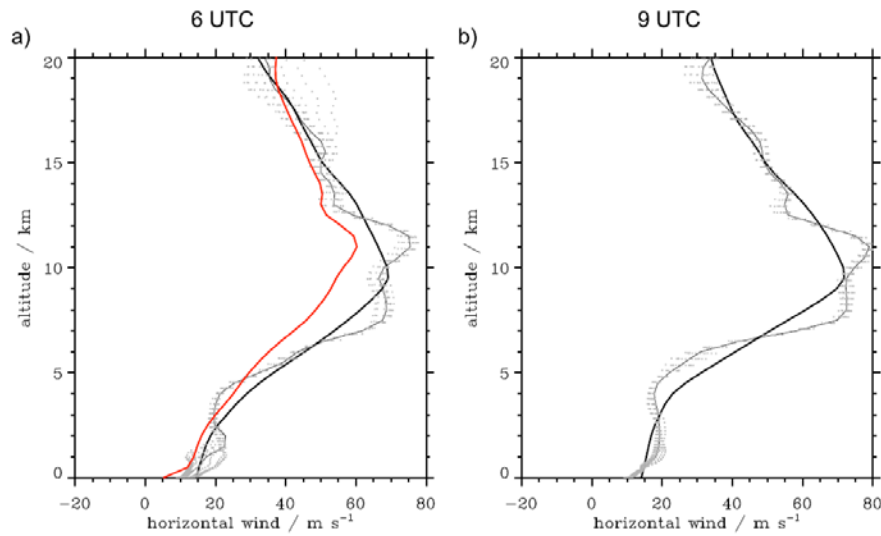


Fig. 2: Vertical profiles of the horizontal wind speed at 42°N for (a) 0600 and (b) 0900 UTC from IFS cycle 41r2 forecasts. Thin lines are calculated on the 500-m vertical grid points, and thick lines are the vertical mean over a 10-km boxcar average. The grey dots show the variability between 108 and 11.58E. The red profile at 0600 UTC shows the T21 profile calculated on the 500-m vertical grid points used to initialize EULAG.

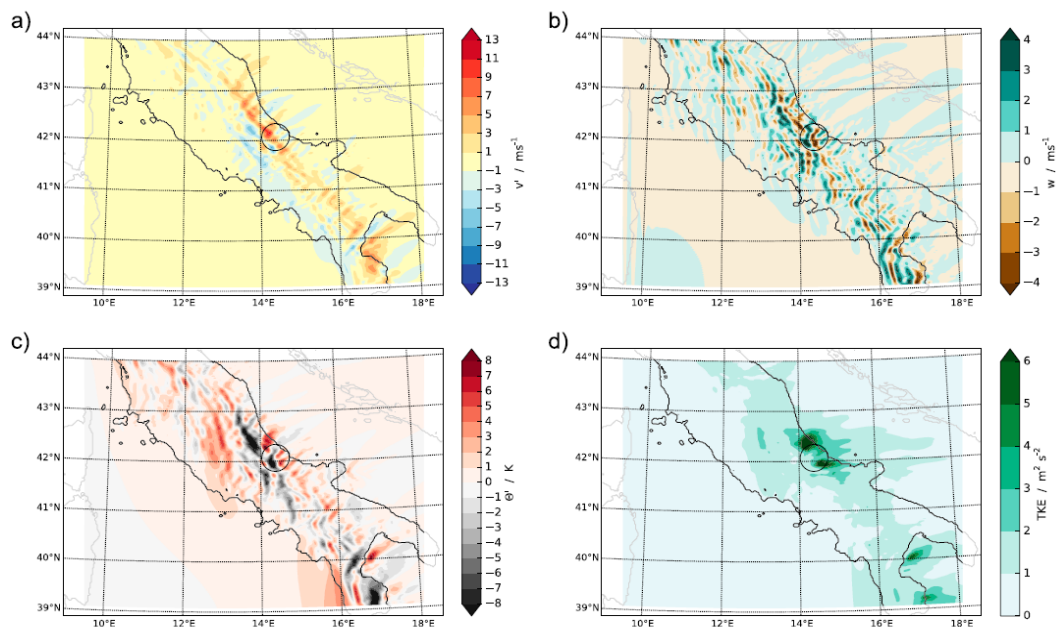


Fig. 3: (a) Meridional wind perturbations, (b) vertical wind, (c) temperature perturbations, and (d) TKE as simulated by EULAG at 12.5 km altitude. The black circle indicates the position of the stall-warning event with a radius of 30 km.

In the region of the stall-warning event (Fig. 3, black circle), short-scale fluctuations with large amplitudes are present in all three parameters. The profiles in Fig. 4 show a decrease in the meridional wind speed from about 10 to -8 m/s within a horizontal distance of approximately 40 km at the altitude range of the flight track. The distance between the maximum and minimum values in the meridional direction is larger by about 10 km relative to the observations. The peak-to-peak amplitude, on the other hand, is, at 18 m/s, slightly smaller than the observed one of about 23 m/s but higher than the amplitude provided by the IFS forecasts. The potential temperature decreases in the same area by about 10 K. Enhanced TKE (Fig. 3d) suggests partial breaking of smaller scale mountain waves above Italy.

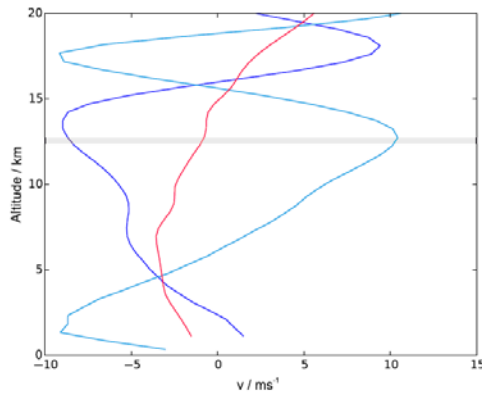


Fig. 4: Vertical profiles of the meridional wind at the positions of the maximum or minimum meridional wind perturbation within the black circle shown in Fig. 3 (blue lines). The red line shows the background meridional wind profile, and the grey shading highlights the altitude of the flight track. The spatial horizontal distance between the blue profiles is about 40 km.

Mountain wave event over Southern Scandinavia

In-situ data at different flight altitudes and downward pointing Doppler wind lidar measurements revealed pronounced changes of the horizontal scales in the vertical velocity field and of the leg-averaged momentum fluxes (MF) in the UTLS region during the mountain wave event (Fig. 5 and Fig. 6). Horizontal scales were 5-9 km at the tropopause inversion layer (TIL) and 10-30 km in the troposphere (Fig. 5d).

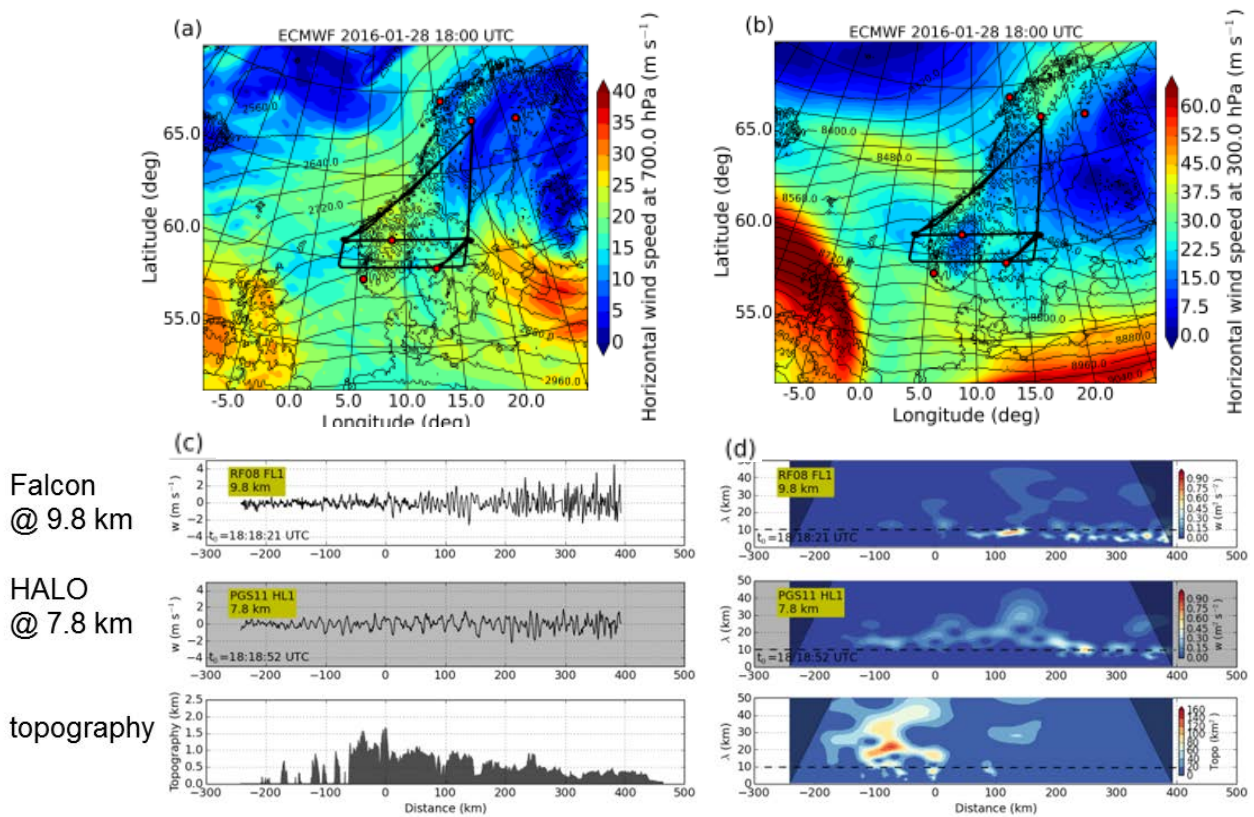


Fig. 5: Meteorological maps of horizontal wind speed and geopotential height (black contour lines) at (a) 700 hPa and (b) 300 hPa at 18 UTC on 28 January 2016 obtained from the ECMWF model. Black lines indicate flight legs of the research flights. Cross mountain flight legs of Falcon and HALO for (c) in-situ vertical wind and topography and (d) corresponding wavelets of vertical wind.

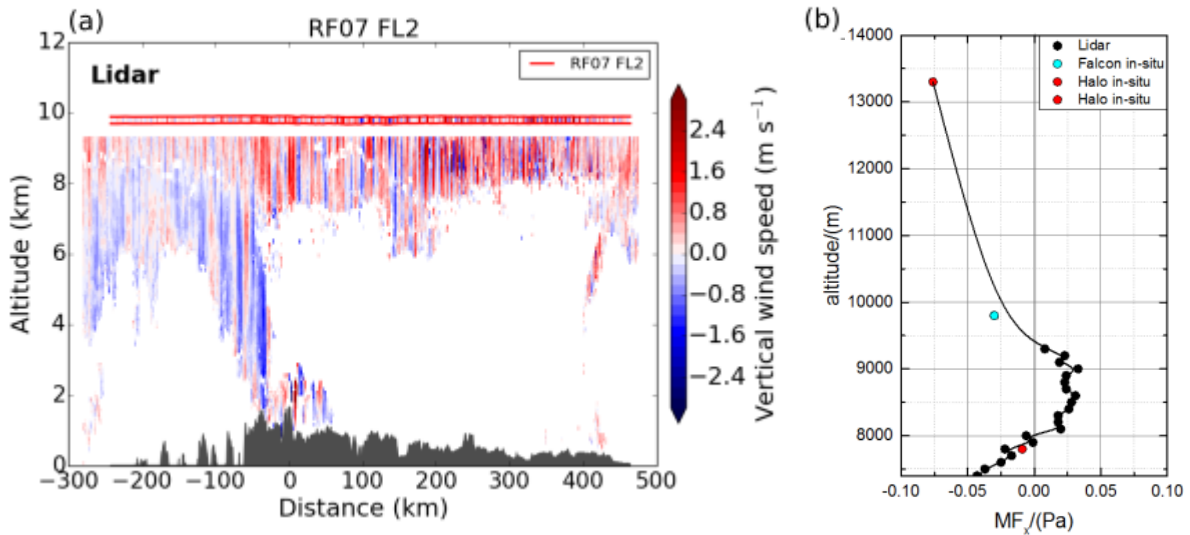


Fig. 6: (a) Vertical winds along flight leg RF07 FL2 measured by the DWL and in-situ instruments (marked by red horizontal lines) at flight level by the DLR Falcon. (b) Leg-integrated momentum flux profile along flight leg RF08 FL2 obtained from DWL measurements and in-situ data.

Although the horizontal scales are around ten kilometres, which is similar to the T-REX observations (Smith et al., 2008; Woods and Smith, 2010), neither Kelvin-Helmholtz instability nor downward propagation of secondary GWs generated by MW breaking in the middle stratosphere are likely able to explain our observations. The vertical shear was not as pronounced as during the T-REX case (Mahalov et al., 2011) because the tropopause jet was not well established over Southern Scandinavia on 28 January 2016 and the wind speed influenced by the large scale mountain wave was only between 10 and 40 m s^{-1} . A mesoscale simulation with the WRF model does not show any indications for wave breaking in the stratosphere over Southern Scandinavia on 28 January 2016. Moreover, the stratospheric critical horizontal wavelengths calculated from co-located radiosonde measurements are larger than the observed scales in the UTLS region which would hinder their downward propagation from a breaking region located higher up.

The concept of interfacial waves on atmospheric inversions can be a possible explanation of such observations in the absence of Kelvin-Helmholtz instabilities and MW breaking in the middle stratosphere. Linear theory is able to describe the horizontal wavelength and the propagation of the interfacial waves (Vosper, 2004; Sachsperger et al., 2015). It is tested if this wave trapping was possible on 28 January 2016 over Southern Scandinavia by performing 2-dimensional simulations with the Scandinavian topography and background profiles which approximate the prevailing conditions on 28 January 2016.

The simulations use a 2-dimensional domain with 2016 and 1000 grid points in x and z directions, respectively, with grid increments of $\Delta x = 500$ m and $\Delta z = 40$ m. This results in a total domain size of about $1008 \text{ km} \times 40 \text{ km}$. The integration time step Δt is set to 1 s. Open boundaries are applied in x -direction. The model top is a rigid lid. The sponge layers at the horizontal edges of the domain are 40 km wide and the sponge layer at the top of the domain starts at 25 km altitude. The Scandinavian topography is interpolated on the 500 m grid from ASTER data. The initial profiles approximate the background conditions over Southern Scandinavia revealed by the Stavanger radiosonde on 28 January 2016 (Fig. 7a, b, d, e). Simulations without and with a TIL are performed. The simplified initial horizontal velocity profile does not contain negative

shear above the tropopause but negative shear of around 8 m s^{-1} establishes in the course of the simulation over the complex topography (black dashed profiles shown in Fig. 7a, d are centred at 100 km distance (Fig. 7c) 16 hours after start of the simulations).

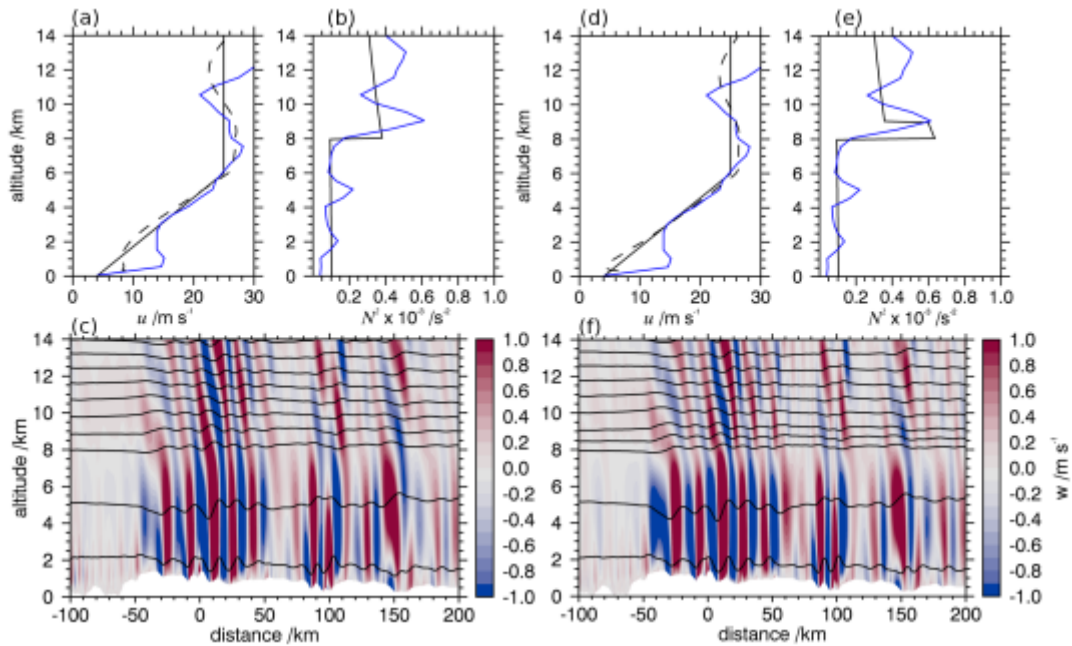


Fig. 7: Initial profiles (black solid) and vertical velocity for the simulations with more realistic terrain and without TIL (a-c) and with TIL (d-f). The initial profiles approximate the background conditions over southern Scandinavia on 28 January 2016 (blue profiles show the Stavanger radiosonde data). Negative shear above the tropopause establishes in the course of the simulations over the mountain range (a, d; black dashed, time = 16 h, distance = 100 km). c and f only show a part of the domain.

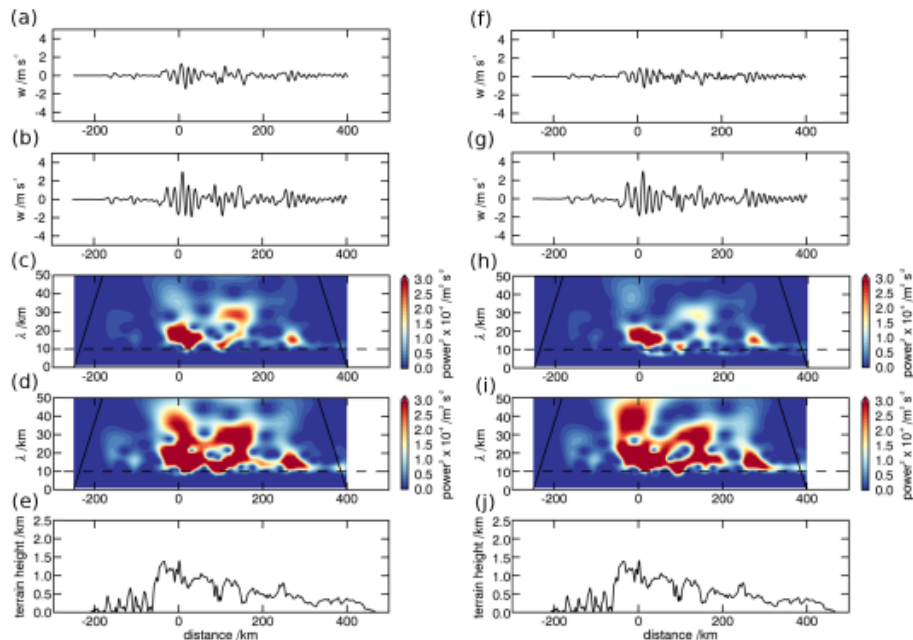


Fig. 8: Vertical velocity and according wavelet spectra of the simulations shown in Fig. 14 (left: without TIL, right: with TIL) in the vicinity of (a, c, f, h) and below (b, d, g, i) the tropopause (inversion). e and j show the terrain in the domain.

Figures 7f and 8h show that interfacial waves can also exist for the background conditions found on 28 January 2016 over Southern Scandinavia. They are found downstream of the main mountain peaks in the vicinity of the TIL (Fig. 7f and Fig. 8f) and their horizontal wavelength is approximately 8 km (Fig. 8h). They

are absent in the troposphere below the TIL (Fig. 8i) and in the case of no TIL (Fig. 7c and Fig. 8a, c). Reflected waves with horizontal wavelengths between 10 and 30 km exist downstream of the main mountain peaks in the troposphere (Figs. 7c, f and 8d, i). These 2-dimensional simulations reveal the expected wavelength of the GWs over Southern Scandinavia downstream of the main mountain ridge on 28 January 2016, i.e. approximately 8 km in the vicinity of the TIL and between 10 and 30 km in the troposphere. However, the interfacial waves in the simulation are not as dominant as in the measurements (Fig. 8h vs. RF08 FL1 in Fig. 5b). There is a stronger signal of the upward propagating MWs above the main mountain peaks (Fig. 8f, h). The amplitudes of interfacial waves depend on the amount of energy provided by the main wave source at the interface and the acting nonlinear processes (Sachsperger et al., 2017). It was not yet investigated how the interaction and generation processes depend on the model resolution and if the amplitudes increase with increasing resolution. The simulations were only 2-dimensional in a Boussinesq framework so they cannot capture effects of the fully 3-dimensional mountain range and increasing MW amplitudes with altitude. Moreover, potential additional energy input by downward propagating larger scale waves from stratospheric sources [e.g., polar night jet (Dörnbrack et al., 2018)] are not included in the simulations. The evaluation of these effects and the assessment of their sensitivities require additional extensive model simulations should be addressed in future studies.

References:

- Amante, C., and B. W. Eakins, 2009: ETOPO1 1 Arc-Minute Global Relief Model: Procedures, data sources and analysis. NOAA National Geophysical Data Center, 19 pp.
- Bramberger, M., A. Dörnbrack, H. Wilms, S. Gemsa, K. Raynor, and R. Sharman, 2018: Vertically Propagating Mountain Waves — A Hazard for High-Flying Aircraft?. *J. Appl. Meteor. Climatol.*, **57**, 1957–1975, <https://doi.org/10.1175/JAMC-D-17-0340.1>
- Dörnbrack, A., Gisinger, S., Kaifler, N., Portele, T. C., Bramberger, M., Rapp, M., Gerding, M., Söder, J., Žagar, N., and Jelic, D.: Gravity waves excited during a minor sudden stratospheric warming, *Atmospheric Chemistry and Physics*, 18, 12915–12931, doi:10.5194/acp-18-12915-2018, 2018.
- Mahalov, A., Moustauoui, M., and Grubišić, V.: A numerical study of mountain waves in the upper troposphere and lower stratosphere, *Atmospheric Chemistry and Physics*, 11, 5123–5139, doi:10.5194/acp-11-5123-2011, 2011
- Sachsperger, J., Serafin, S., and Grubišić, V.: Lee Waves on the Boundary-Layer Inversion and Their Dependence on Free-Atmospheric Stability, *Front. Earth Sci.*, 3, 70, doi:10.3389/feart.2015.00070, 2015
- Sachsperger, J., Serafin, S., Grubišić, V., Stiperski, I., and Paci, A.: The amplitude of lee waves on the boundary-layer inversion, *Quarterly Journal of the Royal Meteorological Society*, 143, 27–36, doi:10.1002/qj.2915, <https://rmets.onlinelibrary.wiley.com/doi/abs/10.1002/qj.2915>, 2017.
- Smith, R. B., Woods, B. K., Jensen, J., Cooper, W. A., Doyle, J. D., Jiang, Q., and Grubišić, V.: Mountain Waves Entering the Stratosphere, *J. Atmos. Sci.*, 65, 2543–2562, doi:10.1175/2007JAS2598.1, 2008.
- Woods, B. K. and Smith, R. B.: Energy Flux and Wavelet Diagnostics of Secondary Mountain Waves, *J. Atmos. Sci.*, 67, 3721–3738, doi:10.1175/2009JAS3285.1, 2010
- Vosper, S. B. (2004), Inversion effects on mountain lee waves. *Q.J.R. Meteorol. Soc.*, **130**: 1723–1748. doi:10.1256/qj.03.63